

Article

Adaptive Fuzzy Power Management Strategy for Extended-Range Electric Logistics Vehicles Based on Driving Pattern Recognition

Changyin Wei ^{1,*}, Xiaodong Wang ², Yunxing Chen ¹ , Huawei Wu ¹ and Yong Chen ^{3,4} 

- ¹ Hubei Key Laboratory of Power System Design and Test for Electrical Vehicle, School of Automotive and Traffic Engineering, Hubei University of Arts and Science, Xiangyang 441053, China; chenyunxing@chd.edu.cn (Y.C.); whw_xy@hbuas.edu.cn (H.W.)
- ² School of Mechanical Automation, Wuhan University of Science and Technology, Wuhan 430081, China; 202203601016@wust.edu.cn
- ³ School of Mechanical Engineering, Guangxi University, Nanning 530004, China; chen Yong1585811@163.com
- ⁴ Tianjin Key Laboratory of New Energy Automobile Power Transmission and Safety Technology, School of Mechanical Engineering, Hebei University of Technology, Tianjin 300130, China
- * Correspondence: weia2@163.com

Abstract: The primary objective of an energy management strategy is to achieve optimal fuel economy through proper energy distribution. The adoption of a fuzzy energy management strategy is hindered due to different reasons, such as uncertainties surrounding its adaptability and sustainability compared to conventional energy control methods. To address this issue, a fuzzy energy management strategy based on long short-term memory neural network driving pattern recognition is proposed. The time-frequency characteristics of vehicle speed are obtained using the Hilbert–Huang transform method. The multi-dimensional features are composed of the time-frequency features of vehicle speed and the time-domain signals of the accelerator pedal and brake pedal. A novel driving pattern recognition approach is designed using a long short-term memory neural network. A dual-input and single-output fuzzy controller is proposed, which takes the required power of the vehicle and the state of charge of the battery as the input, and the comprehensive power of the range extender as the output. The parameters of the fuzzy controller are selected according to the category of driving pattern. The results show that the fuel consumption of the method proposed in this paper is 5.8% lower than that of the traditional fuzzy strategy, and 4.2% lower than the fuzzy strategy of the two-dimensional feature recognition model. In general, the proposed EMS can effectively improve the fuel consumption of extended-range electric vehicles.

Keywords: power management strategy; driving pattern recognition; fuzzy control; extended-range electric logistics vehicle



Citation: Wei, C.; Wang, X.; Chen, Y.; Wu, H.; Chen, Y. Adaptive Fuzzy Power Management Strategy for Extended-Range Electric Logistics Vehicles Based on Driving Pattern Recognition. *Actuators* **2023**, *12*, 410. <https://doi.org/10.3390/act12110410>

Academic Editor: Zhuming Bi

Received: 7 October 2023

Revised: 29 October 2023

Accepted: 1 November 2023

Published: 3 November 2023



Copyright: © 2023 by the authors. Licensee MDPI, Basel, Switzerland. This article is an open access article distributed under the terms and conditions of the Creative Commons Attribution (CC BY) license (<https://creativecommons.org/licenses/by/4.0/>).

1. Introduction

The ongoing evolution of vehicle powertrain is primarily associated with the transition from conventional fossil energy to new energy sources such as hydrogen and electricity, impacting environmental considerations [1,2]. This transition necessitates innovative solutions to deal with the challenge arising from long-distance operations without frequent recharging. The growing concern for environmental sustainability and the need to reduce greenhouse gas emissions have led to the increased development and adoption of electric vehicles (EVs) [3]. In particular, extended-range electric logistics vehicles (ERELVs) have gained attention due to their potential to address the limitations of pure electric vehicles by incorporating an auxiliary power source, such as an internal combustion engine or a fuel cell. The integration of these power sources allows for an extended driving range and improved operational flexibility.

ERELVs offer increased flexibility by incorporating multiple power sources to meet their energy requirements. These sources include a combination of a diesel engine, an

electric motor with a battery, and a fuel cell. Moreover, ERELVs utilize regenerative braking technology to generate electricity during deceleration, which can be stored in the battery. Consequently, ERELVs enhance fuel efficiency and minimize exhaust emissions [4,5]. However, due to the diverse range of energy sources in ERELVs, it is crucial to develop energy management strategies (EMSs) that enable the intelligent coordination and optimization of these sources. The objective is to achieve optimal fuel economy by monitoring the engine's operation within its optimal range, prolonging battery life, reducing CO₂ emissions, and effectively adapting to uncertainties and complex driving conditions [6,7]. To accomplish these objectives, the EMSs in ERELVs require access to real-time information about the driving conditions. This information can be obtained from various sources such as internet maps, global positioning systems (GPS), geographical information systems (GIS), or intelligent transportation systems (ITS) [8]. By integrating these data sources into the EMSs, ERELVs can make informed decisions regarding power allocation, optimizing the utilization of available energy sources, and adapting to the specific driving conditions in real time. This intelligent coordination and management of energy sources contribute to maximizing the overall efficiency and performance of ERELVs in terms of fuel economy and environmental sustainability.

1.1. Literature Review

Effective power management strategies are crucial for optimizing the performance and efficiency of ERELVs. Energy management strategies (EMSs) for vehicle power systems often involve the coordination and allocation of power among multiple power sources through manually set threshold values [9,10]. However, due to the fixed nature of these thresholds, it is difficult to adapt to the nonlinear characteristics of the vehicle system under changing operating conditions, resulting in suboptimal control performance [11]. To address this issue, various optimized energy management strategies have been proposed. Representative EMSs include rule-based energy management strategies (RB-EMSs) and optimization-based energy management strategies [12].

In rule-based energy management strategies, the parameter values in precise logical rules or fuzzy rules are mainly determined by empirical knowledge or the application of optimization methods. While an RB-EMS can provide real-time calculations, its control performance heavily relies on the engineer's experience. Minjae et al. [13] devised a hybrid thermostat energy management strategy for a series hybrid system. Engine output power and speed are determined by the state of charge (SOC) and required power while ensuring that the engine is operating at the optimal curve. Wassif et al. [14] put forward a rule-based real-time energy management strategy with variable thresholds. Three modes of the power system are defined: load balancing, load following, and load mixing. Economical driving control in different modes is achieved based on the driving status change threshold. To solve the problem of computational efficiency, Nicolas et al. [15] proposed a power-following strategy based on genetic algorithm. The results show that the genetic algorithm has a shorter calculation amount and the control effect is close to optimal under various working conditions. Deterministic rule-based energy management strategies cannot fully utilize hybrid powertrains. Many empirically determined parameters still have room for optimization [16]. In order to further improve the efficiency and performance of the deterministic rule energy management strategy, the results of the DP algorithm can be used to inform the formulation of the rule strategy [17]. In optimization-based energy management systems, the energy allocation in hybrid power systems aims to minimize fuel consumption locally or globally [18,19]. Optimization-based EMSs offer good fuel economy and adaptability to driving cycles, but their computational complexity often limits their implementation in whole vehicles. On the other hand, fixed threshold values in rule-based strategies make it challenging to adapt to varying vehicle operating conditions or maintain stable battery state of charge, resulting in suboptimal control [20].

The application of fuzzy intelligent control methods does not rely on high-precision mathematical models, and offers real-time performance and robustness [21]. Therefore, fuzzy

logic-based energy management strategies have broad prospects for application in multi-power source systems [22]. However, their performance heavily relies on the formulation of fuzzy rules, which depends on expert knowledge. These rules can only be optimized for specific operating conditions during design, which may not yield satisfactory control performance in real-world complex and dynamic road conditions. Traditional approaches often rely on rule-based or optimization-based methods, which may not fully adapt to the dynamic nature of real-world driving conditions [23]. Moreover, these strategies often overlook the influence of driving pattern recognition on the power management system [24].

1.2. Motivation and Innovation

As previously discussed, a critical challenge in driving pattern recognition lies in seamlessly integrating the forecasted driving cycle with the power allocation strategy, all the while avoiding the burden of complex frameworks and extensive computational demands. This paper presents a novel approach to power management in ERELVs by incorporating driving pattern recognition and adaptive fuzzy logic techniques. The proposed strategy has the potential to significantly enhance the operational efficiency and sustainability of extended-range electric logistics vehicles, contributing to the advancement of electric transportation.

1.3. Article Overview

This paper is organized as follows: the system description and modeling of the ERELV are described in Section 2. An adaptive fuzzy power management strategy design is proposed in Section 3. Results and discussion are carried out in Section 4, and conclusions are given in Section 5.

2. ERELV Powertrain Modelling

2.1. Vehicle Structure and Longitudinal Dynamics Model

ERELV refers to a series PHEV designed for logistics and transportation purposes, known for its extended range capabilities [25]. Its powertrain system includes a three-cylinder engine, battery pack, electric motor, inverter, and generator, as shown in Figure 1a. The electrical energy in the battery comes from engine power generation, braking energy recovery, and external charging. As there is a decoupling of the mechanical connection between the three-cylinder engine and the wheel, the engine's high efficiency and low emissions region could be tracked properly.

The vehicle longitudinal dynamics model [26] is as shown in Figure 1b. The physical representation of the vehicle is illustrated in Figure 1c. The model parameters of the ERELV are listed in Table 1. The driving torque in motion as a function of the rolling resistance coefficient f and the coefficient of aerodynamic drag C_D is as follows:

$$\eta_T \cdot i_T \cdot T_P + T_b = (m\delta \frac{dv}{dt} + mg \cos \alpha \cdot f + mg \sin \alpha + \frac{1}{2} \rho_a v^2 C_D S) \cdot r_{roll} \quad (1)$$

where m is the overall mass of vehicle, S is the frontal area, and r_{roll} is the rolling radius.

Table 1. ERELV basic parameters.

Components	Description	
Final reduction drive	Final ratio	6.143
Engine	Maximum power (kW)	108
Electric machine	Maximum power (kW)	100
Battery	Rate capacity (Ah)	37
	Vehicle mass (kg)	6000
	C_D	0.335
	S (m ²)	2
Vehicle	Roll coefficient	0.0125
	Wheel radius (m)	0.376
	Rotational mass coefficient	1.06

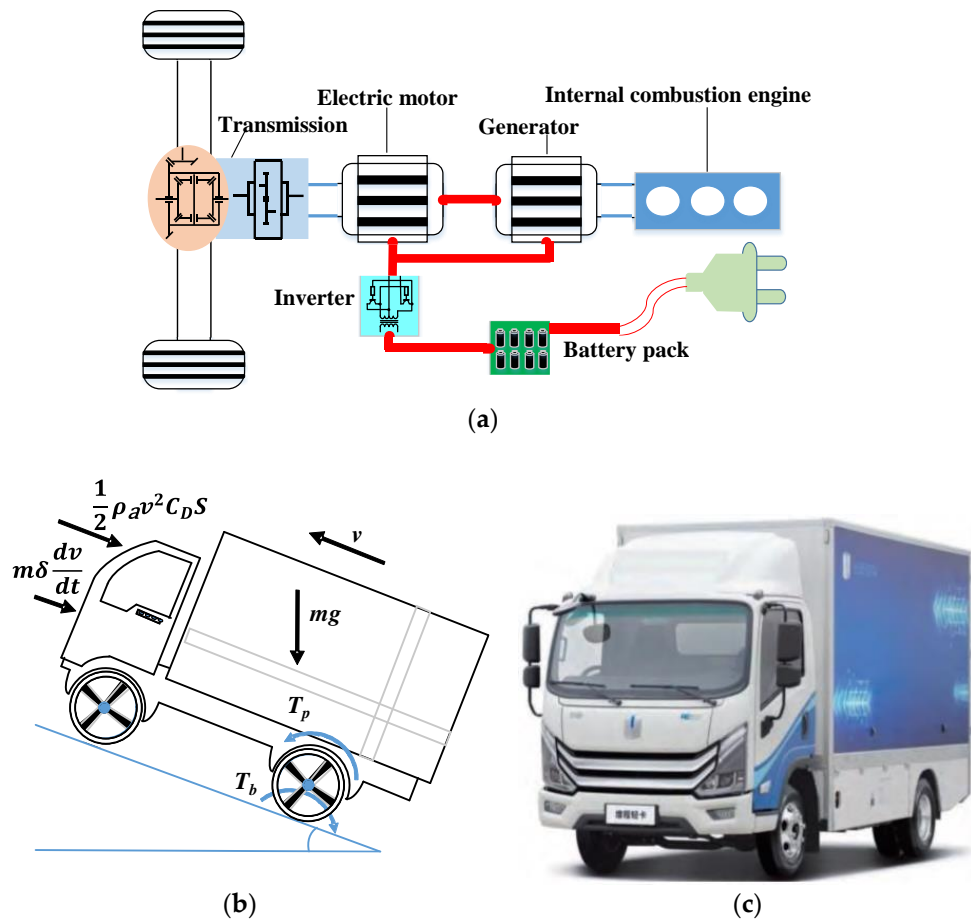


Figure 1. Schematic diagram of (a) hybrid powertrain structure; (b) forces on a vehicle in motion; and (c) vehicle.

2.2. Engine Model

Three-cylinder engines are considered as a promising power generator of the range extender, as a result of their excellent power and high efficiency performance and simple structure, which embedded in the investigated power system. The fuel rate can be defined as a function of the engine efficiency [27]. In addition, fuel consumption Q_e is derived from the following equation:

$$Q_e = \int_{t_1}^{t_2} \frac{T_E(t) \cdot \omega_E(t) \cdot b_E(t)}{1000\rho_f} dt \tag{2}$$

2.3. Electric Machine Model

In extended-range electric vehicles, the motor is the component that provides power. The efficiency of the drive motor is derived from a look-up table, with motor efficiency test data sourced from the literature [24]. The correlation among motor energy consumption Q_f , speed, and torque is described by the following equation:

$$Q_f = \int_{t_1}^{t_2} T_M(t) \cdot \omega_M(t) \cdot \eta_M^{\text{sgn}(T_M)} dt \tag{3}$$

2.4. Battery Model

The electrochemical reaction of the power battery charge–discharge is an importantly complicated process, but the charge–discharge process is simplified to the Rint model including ideal voltage source and internal resistance [28,29]. The state of charge (SOC) is a

function of initial SOC_{init} , open circuit voltage U_{VOC} , and battery internal resistance R_B , and can be defined by the following equation:

$$SOC(t) = SOC_{init} + \int_{t_0}^t \frac{U_{VOC} - \sqrt{U_{VOC}^2 - 4R_B P_B}}{2R_B Q_B} dt \tag{4}$$

3. Adaptive Fuzzy Power Management Strategy

3.1. Driving Pattern Recognition Based on Multi-Dimensional Features

3.1.1. Multi-Domain Feature Extraction Based on the Variational Mode Decomposition Algorithm

Driving pattern recognition is a technology that uses a vehicle-mounted driving state acquisition device to extract features of vehicle speed to identify and match working conditions. It is widely used in energy management systems, driving assistance systems, or intelligent driving systems, and is an important fulcrum for combining AI theory with actual industrial production.

The traditional driving pattern identification method uses manually extracted time-domain vehicle speed driving features for classification, such as average speed, maximum speed, average acceleration, and other time-domain features. Commonly used traditional pattern recognition methods include the Euclidean distance method, similarity distance method, and neural network method. A time-frequency feature extraction method of vehicle speed signals based on Hilbert transform is proposed. The time-frequency characteristic signal and the accelerator pedal and brake pedal signals are jointly constructed to produce multi-dimensional features. The extreme learning machine algorithm and the recurrent neural network are, respectively, integrated to form two multi-dimensional and multi-domain recognition methods. The effects of different parameters, different types of features, and different learning methods on the recognition effect are analyzed. The working condition identification framework based on multi-dimensional features is shown in Figure 2, and a driving database is constructed based on the collected vehicle speeds in typical cities. Multi-dimensional features in the time domain and time-frequency domain are extracted, and a working condition identification model of the sample is constructed under two learning methods.

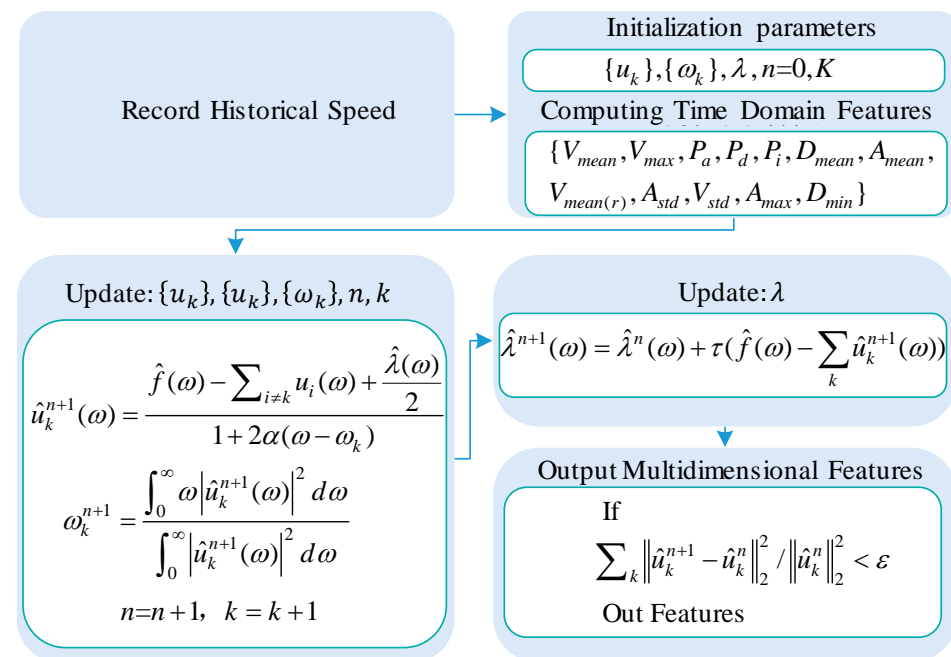


Figure 2. Multi-dimensional feature extraction method framework.

Assuming that the working mode will not change in a short period of time, the historical vehicle speed in a short period of time is selected to identify the current working mode, that is, the historical vehicle speed is selected as the acquisition signal of the working mode recognition method. Statistical methods are used to calculate three time-domain features: average speed, maximum speed, and maximum acceleration. Signal processing principles are used to transform the time-domain signal into a time-frequency-domain signal, and then the time-frequency-domain features are extracted. Hilbert transform proves advantageous in adaptively capturing the time-frequency characteristics of nonlinear historical vehicle speed signals. Its notable feature is the ability to achieve this without the need to select a specific basis function. Additionally, the transformed modal function components exhibit a notable degree of continuity in the frequency domain. Therefore, the variational mode decomposition algorithm (VMD) in Hilbert transform is selected to extract time-frequency features [30].

The multi-dimensional working condition feature extraction method based on VMD is mainly divided into two steps: historical vehicle speed sequence recording and time-frequency feature extraction.

(1) In the offline training recognition model, as many historical vehicle speed data as possible are recorded according to the capacity of the vehicle data storage platform to ensure the accuracy of the recognition model. During online identification, the history window time and update time need to be determined.

(2) The vehicle historical speed is decomposed into intrinsic mode functions (IMF) of different frequency bands using the VMD method. The characteristics of historical vehicle speed signals have a certain degree of randomness and complexity. The time-frequency analysis of vehicle speed is beneficial to achieve control performance. The input vector is the historical 150 s vehicle speed time series, and the elements of the output vector are the operating mode patterns of the next step size of 10 s. Each IMF is assumed to be a finite bandwidth with a center frequency. The variational problem can be described as seeking k modal functions to minimize the sum of the estimated bandwidths of each mode, with the constraint that the sum of each modal function is the original signal [31]. This constrained variation problem is expressed as

$$\begin{aligned} \min_{\{u_k\}\{\omega_k\}} & \left\{ \sum_k \left\| \partial_t \left[\left(\delta(t + \frac{j}{\pi t}) * u_k(t) \right) e^{-j\omega_k t} \right] \right\|_2^2 \right\} \\ \text{s.t.} & \sum_k u_k(t) = f \end{aligned} \tag{5}$$

where ω_k is the center frequency of the k -th mode, and f is the original signal.

The quadratic penalty factor α and the Lagrangian multiplication algorithm λ are introduced to transform the constrained variation problem into an unconstrained variation problem and solve it.

$$\begin{aligned} L(\{u_k\}, \{\omega_k\}, \lambda) & := \alpha \left\{ \sum_k \left\| \partial_t \left[\left(\delta(t + \frac{j}{\pi t}) * u_k(t) \right) e^{-j\omega_k t} \right] \right\|_2^2 \right\} \\ & + \left\| f(t) - \sum_k u_k(t) \right\|_2^2 + \left\langle \lambda(t), s(t) - \sum_k u_k(t) \right\rangle \end{aligned} \tag{6}$$

where k is the Lagrange multiplier.

Applying the multiplier, the alternating direction method iterative update can be expressed as

$$\hat{u}_k^{n+1}(\omega) = \frac{\hat{f}(\omega) - \sum_{i \neq k} u_i(\omega) + \frac{\hat{\lambda}(\omega)}{2}}{1 + 2\alpha(\omega - \omega_k)} \tag{7}$$

$$\omega_k^{n+1} = \frac{\int_0^\infty \omega |\hat{u}_k^{n+1}(\omega)|^2 d\omega}{\int_0^\infty |\hat{u}_k^{n+1}(\omega)|^2 d\omega} \quad (8)$$

where n is the number of iterations.

The Lagrange multiplier update formula is

$$\hat{\lambda}^{n+1}(\omega) = \hat{\lambda}^n(\omega) + \tau(\hat{f}(\omega) - \sum_k \hat{u}_k^{n+1}(\omega)) \quad (9)$$

where $\hat{u}_k^{n+1}(\omega)$ is the Fourier transform of the $n + 1$ iteration of k components. $\hat{\lambda}_k^{n+1}(\omega)$ is the $(n + 1)$ -th Fourier transform of the Lagrange multiplier. The iteration termination condition is

$$\sum_k \left\| \hat{u}_k^{n+1} - \hat{u}_k^n \right\|_2^2 / \left\| \hat{u}_k^n \right\|_2^2 < \varepsilon \quad (10)$$

The process of using variational mode decomposition (VMD) to extract time-frequency features can be summarized in the following steps: (1) Start by initializing the modal functions, instantaneous frequencies, and Lagrangian operators based on the specified number of modal functions, denoted as “ k ”. (2) Enter an iterative loop to update the modal functions, instantaneous frequencies, and Lagrangian operators for each component. The updates are performed according to a specific formula. (3) Continuously evaluate certain conditions to determine whether the convergence criteria have been met. If the conditions are satisfied, exit the iterative loop. (4) Once the convergence criteria are met, the algorithm returns the k modal function components obtained through the iterative process. The framework of the multi-dimensional feature extraction method using VMD is illustrated in Figure 2. The resulting modal components, which represent the time-frequency features extracted from the data, are depicted in Figure 3.

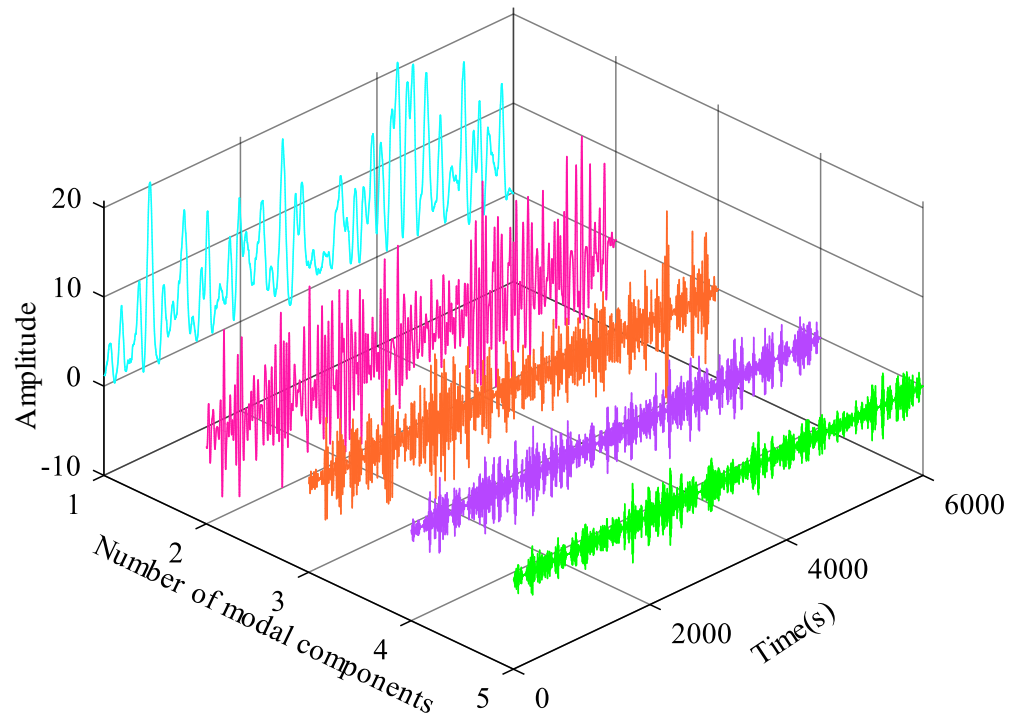


Figure 3. Time-frequency features extracted using the VMD algorithm.

3.1.2. Deep Learning Driving Pattern Identification Method

One of the most widely used methods for addressing time-series classification problems is the recurrent neural network (RNN) [32]. RNNs are designed to capture and store past information and current inputs by introducing state variables, enabling the prediction of current outputs. On the other hand, deep neural networks (DNNs) are an evolution of traditional neural networks, consisting of three main layers: input, hidden, and output. The strength of DNNs lies in their ability to effectively learn and represent complex data patterns. When it comes to working condition pattern recognition, deep neural networks excel at discovering deeper mapping relationships between driving data and patterns of working conditions. In comparison to conventional neural networks, the multi-layer structure of DNNs requires fewer parameters to describe intricate relationships. Consequently, training DNNs with a multi-layer structure tends to be faster and yields better training outcomes.

To balance the requirements of timing signals and computational efficiency while harnessing substantial amounts of data, long short-term memory (LSTM) networks introduce three essential control units: the input gate, the forget gate, and the output gate [33]. These units enhance the influence of historical timing information on current predictions. The network structure of LSTM is depicted in Figure 4. The mathematical expressions for these gate units are as follows:

$$\begin{cases} i_t = \text{sigmoid}(W_i \cdot [h_{t-1}, x_t] + b_i) \\ f_t = \text{sigmoid}(W_f \cdot [h_{t-1}, x_t] + b_f) \\ o_t = \text{sigmoid}(W_o \cdot [h_{t-1}, x_t] + b_o) \end{cases} \quad (11)$$

where the three logic gates are sigmoid. The coefficients are W_i , W_f , and W_o . h_{t-1} is the hidden unit information at the previous moment, x_{t-1} is the input vector, and b_i , b_f , and b_o are deviations.

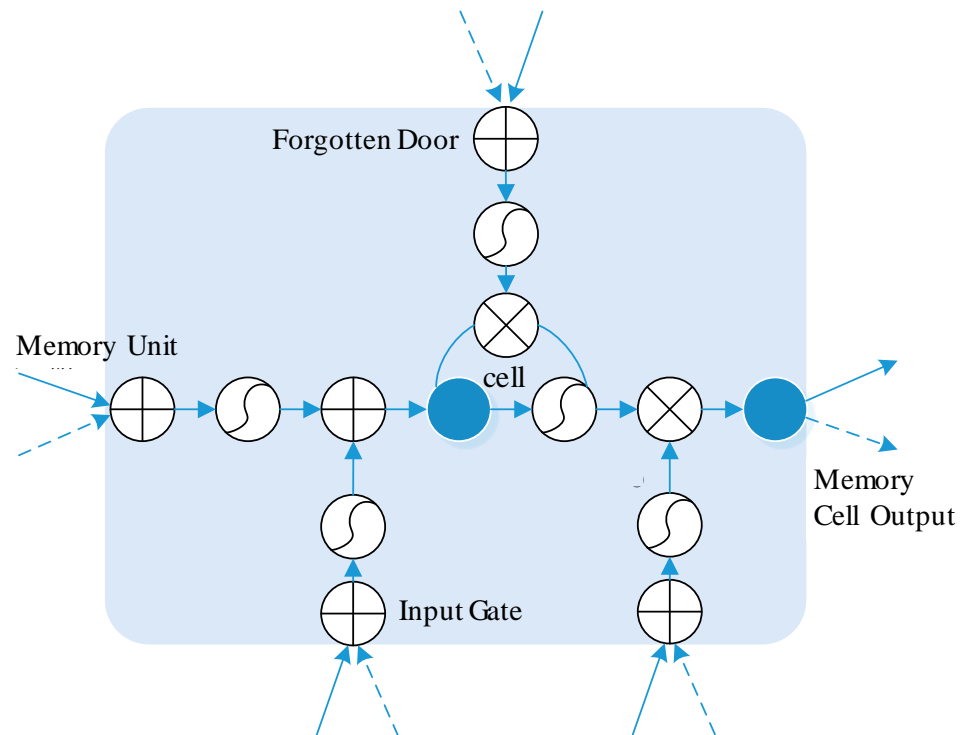


Figure 4. LSTM network structure.

The expression of the alternative information update process of the input gate is [34]

$$\begin{cases} \tilde{C}_t = \tanh(W_e[h_{t-1}, x_t] + b_e) \\ f_t = f_t * C_{t-1} + i_t * \tilde{C}_t \\ h_t = o_t * \tanh(C_t) \end{cases} \tag{12}$$

where the activation function is the tanh function, W_e is the weight matrix, b_e is the deviation of the updated information unit, and C_{t-1} is the information of the memory unit at the previous moment.

The output gate update formula is

$$h_t = o_t * \tanh(C_t) \tag{13}$$

where h_t is the hidden state information at the current moment.

During working mode recognition, the data volume of the input signal of the LSTM neural network will be different from that of the DNN recognition model, but the information included is the historical vehicle speed, accelerator pedal opening, and brake pedal opening, and the output is a different recognition step size. When using the LSTM-NN prediction model to identify the operating mode, the input information and output information are

$$\begin{aligned} Output(t) &= f_{LSTM-NN}(Input) \\ Input(t) &= \left\{ \begin{array}{l} [v_{t-hh+1}, v_{t-hh+2}, \dots, v_{t-1}, v_t] \\ [g_t, g_{t+1}, \dots, g_{t+hp-1}, g_{t+hp}] \\ [a_t] \\ [s_t] \end{array} \right\} \\ Output(t) &= \{v_{t+1}, v_{t+2}, \dots, v_{t+hp}\} \end{aligned} \tag{14}$$

3.2. Adaptive Fuzzy Energy Management Strategy

In an effort to mitigate the energy consumption of extended-range electric vehicles, a dual-input single-output fuzzy controller has been devised [35,36]. As depicted in Figure 5, this fuzzy controller takes into account both the vehicle’s power demand and the battery’s state of charge (SOC) as inputs, yielding the comprehensive power output for the range extender. The purpose of employing the fuzzy rule-based controller is twofold: optimizing engine operation within the high-efficiency region while simultaneously ensuring the stability of the battery SOC.

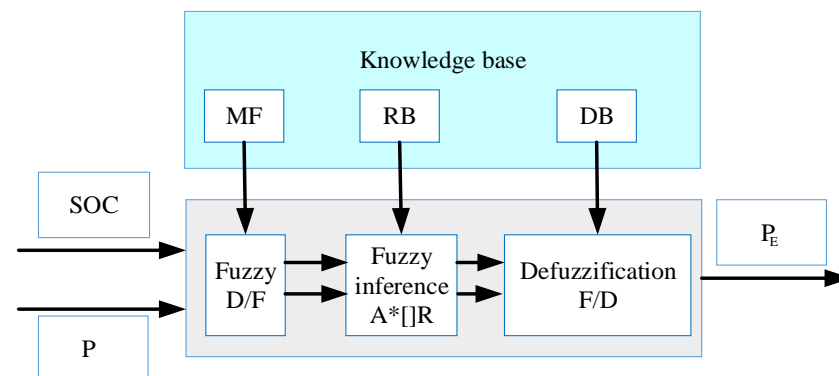


Figure 5. Fuzzy controller structure.

The control process begins by subjecting both the SOC and the required power to a process of fuzzification. Subsequently, the membership degrees of linguistic values are computed by utilizing the rule base and membership functions. Finally, the defuzzification module is employed to translate the fuzzy semantic values into precise control instructions, which are then conveyed to the vehicle’s power system.

The fuzzy control rules utilized are presented in Table 2. The input variables SOC and demand power are each divided into three fuzzy subsets, denoted as {Low (L), Medium (M), High (H)}. On the other hand, the output power is categorized into five fuzzy subsets: {Very Low (VL), Low (L), Medium (M), High (H), Very High (VH)}. The SOC range encompasses values from [0, 1], while the range for required power is [−150, 150].

Table 2. Fuzzy control rules.

Required Power	SOC		
	L	M	H
L	VL	L	M
M	L	M	H
H	M	H	VH

The calculation formula of the trapezoidal membership function is as follows:

$$\mu_F = \begin{cases} 0 & x < a \\ \frac{x-a}{b-a} & a \leq x < b \\ 1 & b \leq x < c \\ \frac{d-x}{d-c} & c \leq x \leq d \\ 0 & x > d \end{cases} \tag{15}$$

The method of defuzzification is the centroid removal method, that is, the output of the fuzzy controller can be obtained using the following formula:

$$u_f(k) = \frac{\sum_{j=1}^{r_1} \sum_{i=1}^{r_2} u_{l_1}^j(k) u_{l_2}^i(k) \Delta u_{ij}(k)}{\sum_{j=1}^{r_1} \sum_{i=1}^{r_2} u_{l_1}^j(k) u_{l_2}^i(k)} \tag{16}$$

where u_f is the fuzzy controller output, and $u_{l_1}^j(k)$ is the membership degree of SOC and demand power.

The membership function input to the fuzzy controller is shown in Figure 6. The performance of the fuzzy controller is mainly affected by the vertex coordinates of the input and output membership functions. Therefore, the 11 vertex coordinates are used as optimization variables, the fuel economy in the power maintenance stage is the optimization target, and the improved genetic algorithm is used as the optimization method.

The optimization variables are the vertex coordinates of the input and output membership functions, and the expression is

$$X = [x_1, x_2, x_3, x_4, x_5, x_6, x_7, x_8, x_9, x_{10}, x_{11}]^T \tag{17}$$

The coordinate position of the vertex of the optimization variable in the formula is shown in Figure 6. Each coordinate should satisfy the following:

$$\begin{cases} x_1 \leq x_2 \leq x_3 \\ x_4 \leq x_5 \leq x_6 \\ x_7 \leq x_8 \leq x_9 \leq x_{10} \leq x_{11} \end{cases} \quad (18)$$

To avoid the impact of electric power on fuel economy evaluation, the fuel consumption during the electric power maintenance phase is selected as the optimization target, and the expression is as follows:

$$J = \min \left(\int_{t_0}^{t_f} m_f(\omega_e(t), T_e(t)) dt \right) \quad (19)$$

where $\omega_e(t)$ and $T_e(t)$ are the engine speed (rad/s) and torque (N·m) changing with time under test conditions; and m_f is the engine fuel consumption rate.

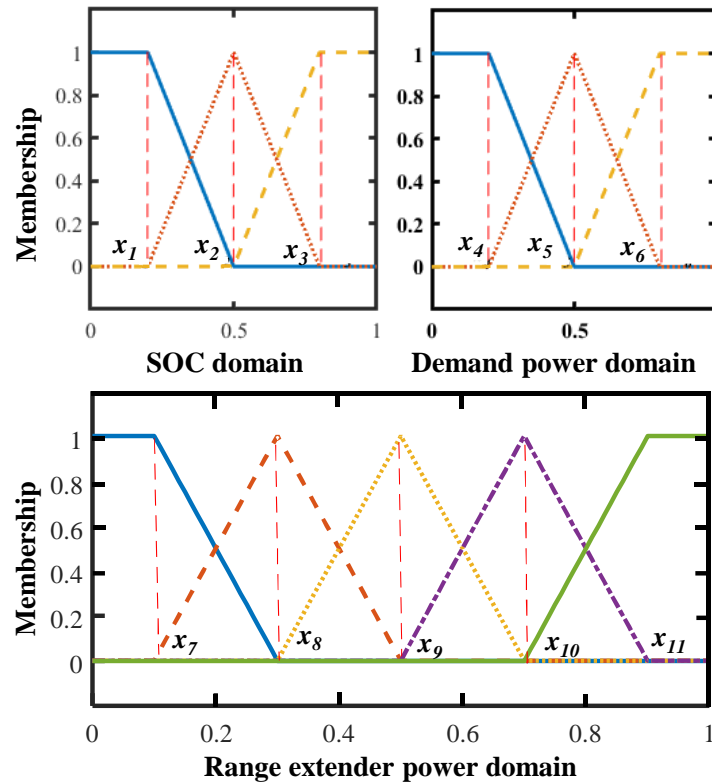


Figure 6. Membership function.

The designed framework for a fuzzy energy management strategy in neural network-based working condition identification is illustrated in Figure 7. It is divided into two key components: offline optimization and online fuzzy real-time control. Urban working conditions data are utilized as training samples to construct a recognition model. This model’s purpose is to identify and classify three types of working conditions. During the power maintenance stage within these working condition cycles, the optimization objective is to minimize fuel consumption. To achieve this, an improved genetic algorithm is employed as the optimization method. The parameters of the fuzzy controller, operating under the three types of working conditions, are optimized offline using this approach. Within the fuzzy real-time control portion of the framework, the optimal parameters

determined during the offline optimization stage are transferred to the controller. The controller takes several inputs, including the required power, state of charge (SOC), and the category of the working condition. After considering these inputs and ensuring compliance with various decision constraints, the fuzzy controller selects the optimal control parameters for real-time decision making. This ensures that the system operates optimally under different working conditions.

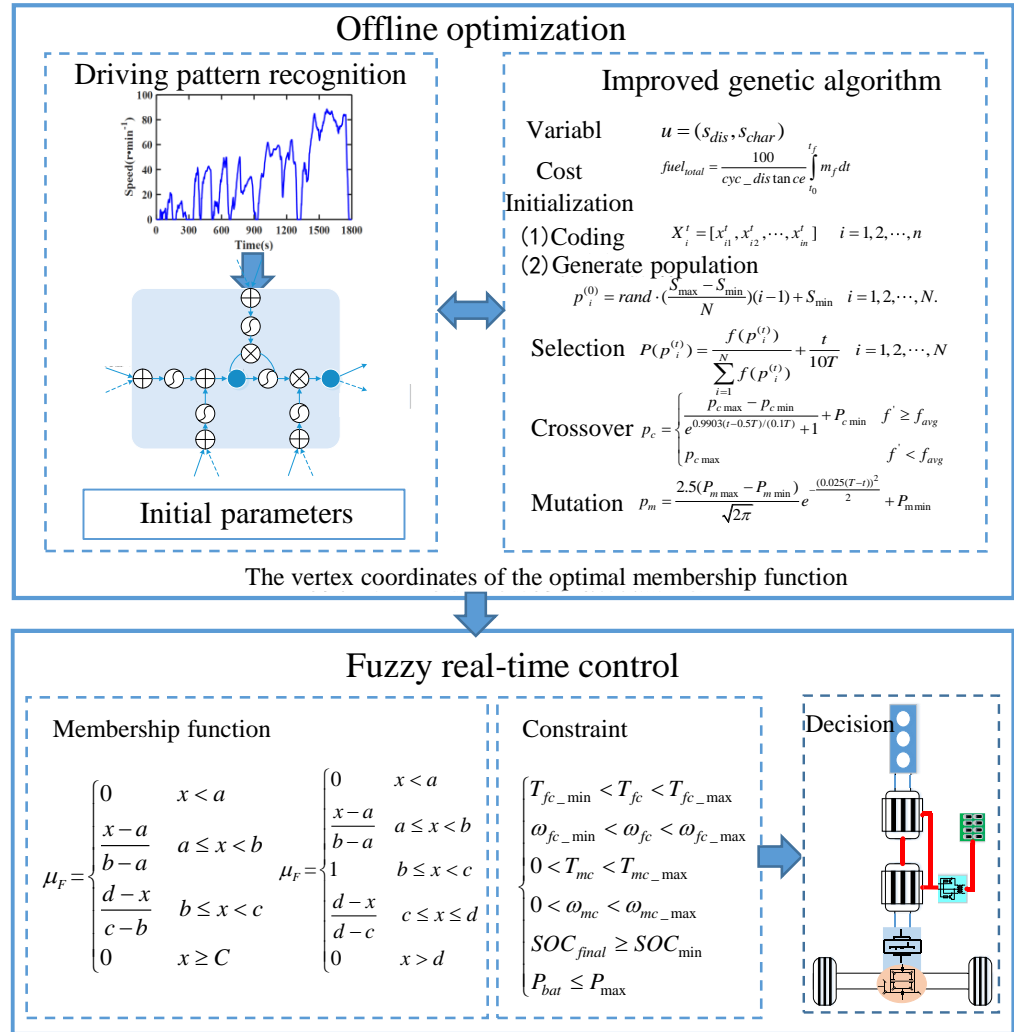


Figure 7. Fuzzy energy management strategy framework for working condition recognition using a neural network.

In summary, this framework combines offline optimization to ascertain optimal fuzzy controller parameters and online fuzzy real-time control to adapt and make optimal decisions based on the current working condition. It is designed to enhance energy management within a neural network-based system, ultimately aiming to minimize fuel consumption and improve overall performance.

4. Results and Discussion

4.1. Driving Pattern Recognition Performance Verification

To validate the efficacy of the method proposed in this article and investigate the influence of various factors and methodologies on its performance, we gathered vehicle speed data in Tianjin City from the literature [37]. Integrating the K-means clustering method, we segmented the data into three kinematic categories: urban, suburban, and expressway. Subsequently, we extracted 5000 s of historical data from each segment to

train the model, as shown in Figures 8 and 9. Figure 10 depicts the extracted accelerator pedal and brake pedal signals for their respective segments. While these three types of features are distinct in each kinematic segment, practical applications necessitate a fixed online identification window time.

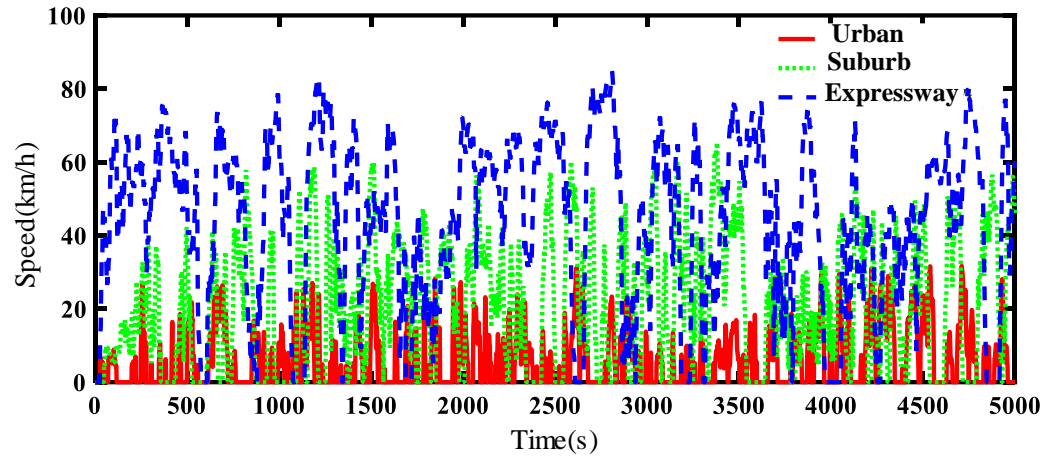


Figure 8. Training data.

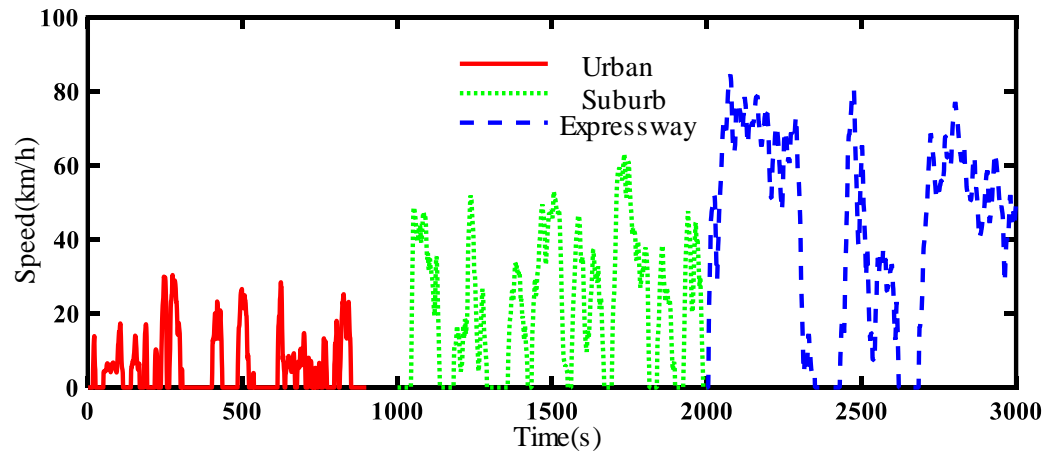


Figure 9. Test data.

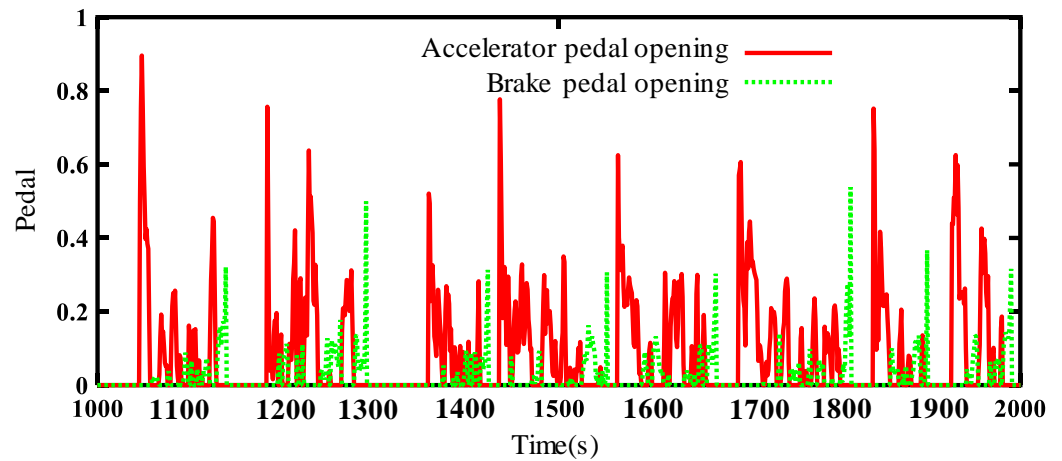


Figure 10. Acceleration and brake pedal opening at 1000 s–2000 s.

During the training phase, we utilized historical vehicle speed data to create training datasets based on the size of the data recording window. The term “update window” pertains to the interval for refreshing driving mode recognition, which is also called the recognition step. For instance, with a total of 5000 s of data and assuming a 150-s recording window and a 10-s update window, we generated 486 samples for the first data type. In total, we constructed 1458 samples across the three categories for training. Additionally, we selected 1000 s of each kinematic segment distinct from the training data to serve as test data. Employing the same 150-s recording window and 10-s update window, we created 258 samples for testing purposes.

Figures 8 and 9 display the velocity contour curves for both the training and test data. In the first type of training data, the sixth kinematic segment exhibits an average speed of 7.60 km/h, a maximum speed of 26.85 km/h, and an average acceleration of 0.65 m/s². Contrastingly, in the second type of training data, the same kinematic segment showcases an average speed of 11 km/h, a maximum speed of 41.60 km/h, and an average acceleration of 0.4988 m/s². These observations underscore the distinct kinematic characteristics between different types. In the third category, the sixth kinematic segment stands out with an average speed of 47.40 km/h, a maximum speed of 76.36 km/h, and an average acceleration of 0.2669 m/s². However, it is crucial to note that when using fixed historical time periods as input for the recognition model in practical applications, the differences in time-domain statistical characteristics may not be readily apparent, leading to lower recognition accuracy. Thus, it becomes imperative to incorporate multi-dimensional and multi-domain features such as time-frequency characteristics, accelerator pedal signals, and brake pedal signals.

Figure 10 illustrates the pedal opening curve ranging from 1000 s to 2000 s. In this graph, the solid line represents the accelerator pedal opening, while the dotted line represents the brake pedal opening. Notably, the average opening of the accelerator pedal surpasses that of the brake pedal. This disparity can be attributed to the distinct roles these pedals play during vehicle operation.

The accelerator pedal primarily controls the driving force of the vehicle and is tasked with overcoming various types of resistance such as air resistance, acceleration resistance, and slope resistance while ensuring smooth acceleration. On the other hand, the brake pedal is involved in the deceleration process, where it contends with two types of resistance: motor energy recuperation, which contributes to braking through energy recovery, and mechanical braking force.

4.1.1. The Impact of Time-Frequency Domain Feature Estimates on Recognition Performance

The term “number of time-frequency domain feature estimates” pertains to the quantity of time-frequency features derived from the time-domain signal through the variational mode decomposition algorithm. To investigate the influence of these estimates on recognition performance, we set the historical driving feature recording window time to 150 s. To assess the effectiveness of recognition, the evaluation relies on both the recognition rate and the overfitting degree. Their definitions are provided below:

$$P_{AC} = \frac{N_C}{N_T} \quad (20)$$

$$D = \frac{P_{AC_train} - P_{AC_test}}{P_{AC_train}} \quad (21)$$

where P_{AC} is the recognition rate, N_C and N_T are the correct classification and the total number, respectively, D is the overfitting degree, and P_{AC_train} and P_{AC_test} are the training recognition rate and the test recognition rate, respectively.

Subsequently, we varied the update time for future working condition pattern recognition to 5 s, 10 s, 15 s, and 20 s, respectively, and assessed the degree of overfitting associated with different estimates ranging from three to nine. The outcomes are presented in Figure 11. Across the four update time intervals, the recognition rate initially ascends

and then declines as the number of estimates increases, with the peak recognition rate occurring when the estimated number is seven. Specifically, the maximum recognition rates at 5 s, 10 s, 15 s, and 20 s are 0.980, 0.973, 0.957, and 0.955, respectively. Conversely, the overfitting degree initially decreases and then increases with an increasing number of estimates. The minimum overfitting degree is observed when there are seven estimates, with corresponding values of 0.020, 0.027, 0.029, and 0.032 under the four update times, respectively. Consequently, the optimal number of time-frequency domain feature estimates is determined to be seven. The recognition rate diminishes as the update time increases. This trend suggests that the longer the update time, the more pronounced the impact on the recognition rate, following an initial rise and fall as the estimated number increases. Additionally, the overfitting degree amplifies with longer update times, with the value initially decreasing and then increasing as the estimate number grows.

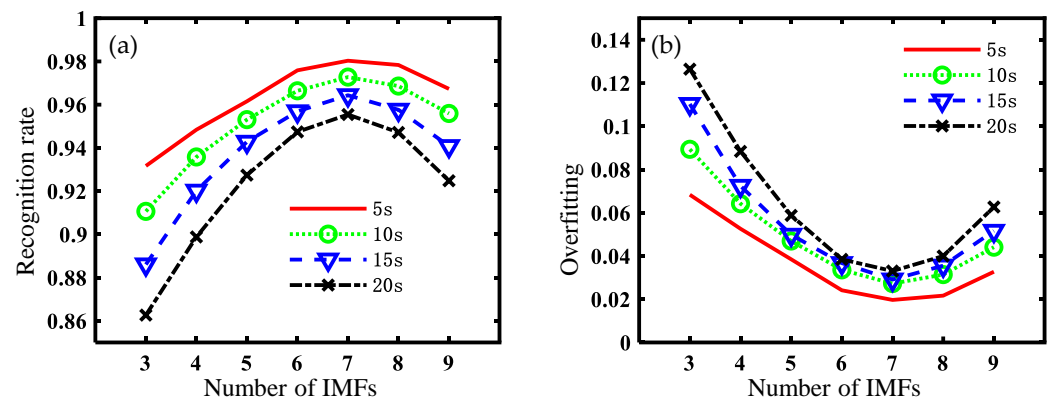


Figure 11. Result comparison under different update times: (a) recognition rate; (b) overfitting.

Moving on to Figure 12, it provides a comparison of recognition performance under various historical driving information recording times. Notably, under the same time-frequency feature estimates, the recognition rate is at its highest and the overfitting degree is at its lowest when the recording time is set to 150 s. This observation underscores that a recording time of 150 s yields the most favorable recognition results among the four time intervals considered.

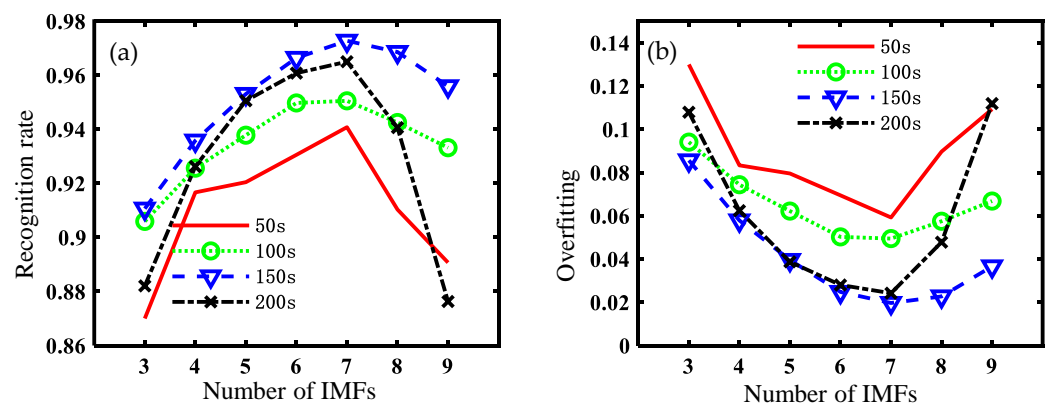


Figure 12. Comparison of results at different recording times: (a) recognition rate; (b) overfitting.

4.1.2. Comparison of the Two Identification Methods

To compare and analyze the performance of the two recognition methods, we calculate the overfitting degree of the recognition rate domain for both methods at recognition step lengths of 5 s, 10 s, 15 s, and 20 s. Table 3 presents the recognition effects of the two learning methods proposed in this article. The table indicates that when the recognition step size is consistent, LSTM exhibits a higher recognition rate than the extreme learning machine

(ELM), and its overfitting degree is lower compared to ELM. Consequently, the recognition effect of LSTM surpasses that of ELM.

Table 3. The recognition effect of different learning methods.

Recognition Step Size	LSTM Recognition Rate	ELM Recognition Rate	LSTM Overfitting Degree	ELM Overfitting Degree
5 s	0.980	0.960	0.020	0.040
10 s	0.973	0.953	0.027	0.047
15 s	0.964	0.940	0.032	0.051
20 s	0.955	0.920	0.031	0.068

4.1.3. The Impact of Different Types of Features on Recognition Performance

Table 4 provides a comprehensive overview of the working condition identification results, considering different feature types and recognition step sizes. These features encompass time-domain attributes (T, including average speed, maximum speed, and average acceleration), time-frequency-domain characteristics (F, derived from the signal post VMD decomposition), accelerator pedal signals (A), and brake pedal signals (B). The recognition steps of 5 s, 10 s, 15 s, and 20 s were utilized, with historical driving information recorded over a 150 s time period. When feature types remain constant, the recognition rate exhibits a decreasing trend as the recognition step size grows larger, accompanied by an escalation in overfitting. For instance, with only time-domain features and a 5 s recognition step, the recognition rate stands at 0.917, with an overfitting degree of 0.083. Increasing the recognition step to 10 s results in a recognition rate of 0.894 and an overfitting degree of 0.101. Extending the step to 20 s leads to a reduced recognition rate of 0.887, accompanied by an increased overfitting degree of 0.113.

Table 4. Recognition results under different types of features.

Feature Type	Recognition Step	Recognition Rate	Overfitting Degree
T	5 s	0.9171	0.0828
	10 s	0.8941	0.1014
	15 s	0.8872	0.1057
	20 s	0.8783	0.1129
T + F	5 s	0.9675	0.0323
	10 s	0.9566	0.0386
	15 s	0.9300	0.0624
	20 s	0.9235	0.0671
T + A	5 s	0.9226	0.0772
	10 s	0.9203	0.0751
	15 s	0.9002	0.0925
	20 s	0.8914	0.0996
T + B	5 s	0.9232	0.0766
	10 s	0.9047	0.0907
	15 s	0.8958	0.0969
	20 s	0.8894	0.1016
T + F + A + B	5 s	0.9803	0.0195
	10 s	0.9728	0.0223
	15 s	0.9644	0.0278
	20 s	0.9554	0.0348

However, maintaining a consistent recognition step size while introducing additional feature types can yield improvements in recognition rate and a reduction in overfitting. For instance, with a 15 s recognition step, the recognition rate for time-domain features alone is 0.887, with an overfitting degree of 0.106. When combining time-domain and time-frequency-domain features, the recognition rate increases to 0.930, with a reduced overfitting degree of 0.062. Similarly, incorporating time-domain features with accelerator pedal signals results in a recognition rate of 0.900 and an overfitting degree of 0.093. The recognition rate under time-domain features combined with brake pedal signals is 0.896,

with an overfitting degree of 0.097. The most significant improvement is achieved when all four features are employed together, yielding a recognition rate of 0.964 and the lowest overfitting degree of 0.028.

Among these features, time-frequency-domain features have the most substantial impact on recognition rate, followed by accelerator pedal signal features, with brake pedal signal features having the smallest influence. Combining time-frequency-domain features, accelerator pedal signals, and brake pedal signals results in the most substantial enhancement in recognition efficiency. In summary, integrating diverse feature types for working condition identification can further elevate the recognition rate and optimize overall performance.

4.2. Performance Comparison of Energy Management Strategies

The fuzzy controller's state of charge (SOC) membership function and demand power vertex coordinate parameters have been optimized. The normalized SOC membership function parameters are [0.4497, 0.8644, 0.9540], while the demand power membership function parameters are [0.8165, 0.7201, 0.1220]. The output membership function parameters are [0.0830, 0.8391, 0.3500, 0.9056, 0.5779]. Table 5 displays the optimal fuzzy controller parameters for three different operating modes. It is evident from the table that the optimal control parameters vary for different operating modes. To assess the effectiveness of the adaptive fuzzy energy management strategy that incorporates working condition identification, a simulation comparison analysis was conducted between the traditional fuzzy energy management strategy and the fuzzy energy management strategy using various working condition identification methods.

Figure 13 illustrates the SOC curves under different strategies. The SOC fluctuations are relatively small in the traditional fuzzy strategy. The difference between the maximum SOC and the minimum SOC is 0.0134. In contrast, the SOC difference of the fuzzy strategy under T + F + A + B is 0.0198, under T + F it is 0.0212, under T it is 0.0237, under T + B it is 0.0218, and under T + A it is 0.0201. This difference is because the traditional fuzzy strategy lacks working condition identification during the power maintenance stage, making it unable to accurately determine the working condition. Consequently, the SOC must be balanced as much as possible at any vehicle speed.

Table 6 clearly demonstrates that the fuel consumption of the traditional fuzzy energy management strategy is 2408 g. When compared to this traditional approach, the fuzzy energy management strategy incorporating multi-dimensional characteristic working condition identification (T + F + A + B) achieves a fuel consumption of 2268 g, resulting in a fuel saving of 5.8%. Similarly, the fuzzy strategy using T + F characteristics achieves a fuel consumption of 2294 g, translating to a fuel saving of 4.7%. For the fuzzy strategy with T characteristics, fuel consumption is 2327 g, offering a fuel saving of 3.4%. When employing the fuzzy strategy with T+B characteristics, fuel consumption totals 2307 g, resulting in a fuel saving of 4.2%. Lastly, the fuzzy strategy with T + A characteristics records a fuel consumption of 2316 g, representing a fuel saving of 3.8%. In terms of engine start time, all of these strategies exhibit reductions of 5.8%, 4.7%, 3.4%, 4.2%, and 3.8%, respectively. Furthermore, the average rate of change of battery power decreases in each case. These results highlight that the fuzzy energy management strategy, when integrated with working condition recognition, can significantly enhance fuel economy during the power maintenance stage. Among the various working condition identification methods based on different types of characteristics, the strategy incorporating multi-dimensional characteristics, encompassing time-domain, time-frequency-domain, accelerator pedal signal, and brake pedal signal data, proves to be the most effective for improving fuel efficiency.

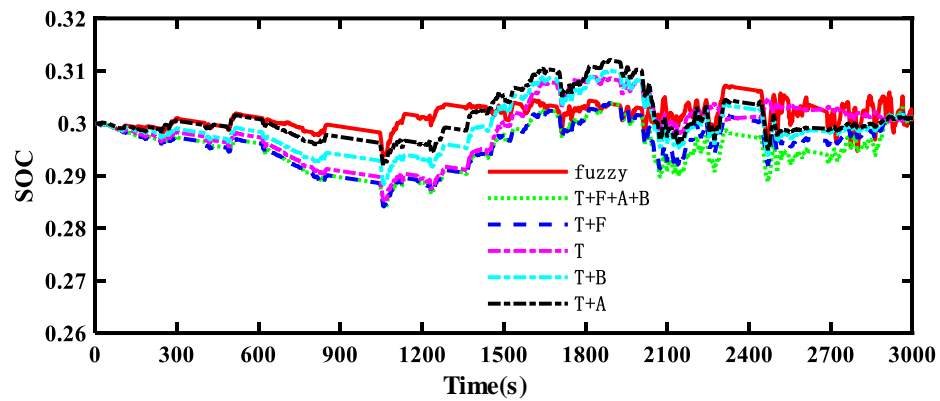


Figure 13. SOC with different strategies.

Table 5. Fuzzy controller parameters under different operating modes.

Abscissa of Vertex	Urban	Suburban	Expressways
x_1	0.7523	0.7336	0.4690
x_2	0.8949	0.3011	0.0873
x_3	0.8418	0.4956	0.8287
x_4	0.1309	0.2582	0.6859
x_5	0.1892	0.7329	0.2673
x_6	0.1536	0.1168	0.9695
x_7	0.0289	0.7460	0.1838
x_8	0.0091	0.8098	0.2999
x_9	0.5965	0.7452	0.4112
x_{10}	0.6090	0.3371	0.2365
x_{11}	0.9189	0.5843	0.1951

Table 6. Performance comparison under different strategies.

Different Strategies	Fuel Consumption (g)	SOC _{end}	Number of Engine Starts	Engine on Time	Average Rate of Change of Battery Power (kw/s)
Fuzzy	2408	0.3013	177	1057	6.67
T + F + A + B	2268	0.3010	165	973	6.48
T + F	2294	0.3014	165	974	6.53
T	2327	0.3007	166	971	6.62
T + B	2307	0.3006	170	1011	6.53
T + A	2316	0.3013	165	983	6.60

Figure 14 presents the distribution of engine operating points under different strategies. It is evident from the figure that all three strategies are operating along the optimal operating curve for range extender efficiency. Since the range extender only provides power according to the strategy, decoupling the range extender’s rotational speed from the vehicle speed allows the operating point to align with the optimal operating curve. The operating point distribution of the fuzzy strategy under the T + F + A + B working condition identification method appears relatively narrow, while the traditional fuzzy power distribution exhibits a wider spread. This distinction arises because the fuzzy energy management strategy, after incorporating working condition identification, reduces the number of operating points in low-efficiency areas. This optimization is aimed at further enhancing fuel economy by avoiding operation in less efficient regions of the engine’s performance curve.

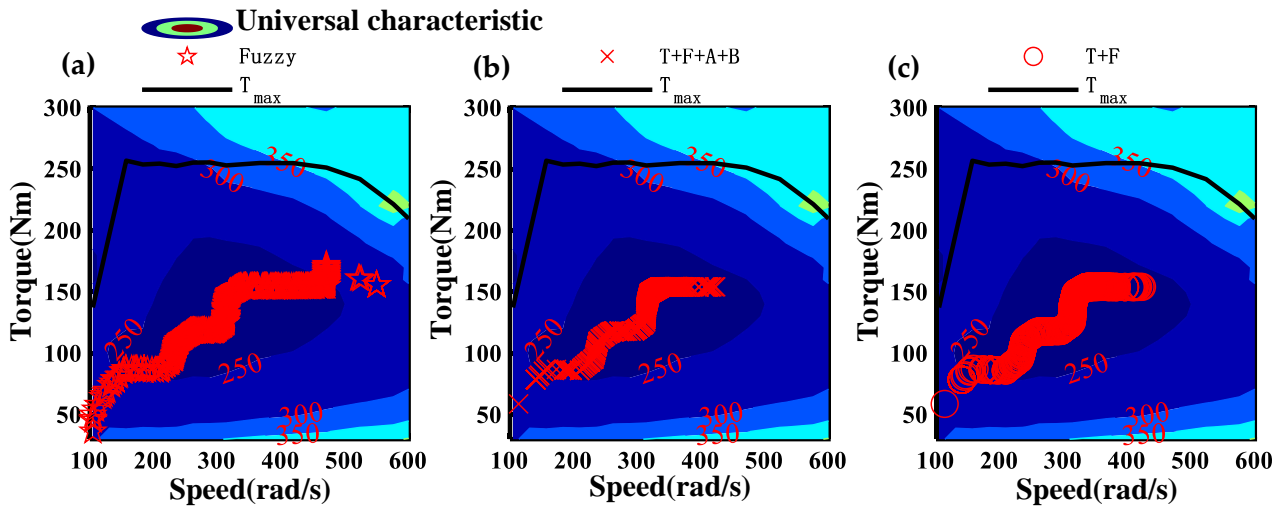


Figure 14. Engine operating point distribution: (a) fuzzy strategy; (b) fuzzy strategy under T + F + A + B features; and (c) fuzzy strategy under T + F features.

To provide a more detailed comparison of fuel economy among the three strategies, the proportion of engine fuel consumption within specific ranges was statistically calculated. The results are presented in Figures 15 and 16. The fuel consumption rate of the traditional fuzzy strategy falls within the range of [220, 240) grams per kilowatt-hour (g/kWh), accounting for 29.32% of the data. Moreover, within the range of [220, 260) g/kWh, the proportion is 68.52%. In contrast, the fuzzy strategy incorporating T + F + A + B working condition identification exhibits a fuel consumption rate within the [220, 240) g/kWh range, accounting for 42.20% of the data. This represents a 12.88% increase compared to the corresponding range of the traditional fuzzy strategy. Additionally, within the [220, 260) g/kWh range, the proportion is 71.82%, which is 3.3% higher than the corresponding range of the traditional fuzzy strategy. These results clearly demonstrate that the fuzzy energy management strategy incorporating T + F + A + B working condition identification achieves the optimal fuel economy among the three strategies, with significantly improved fuel efficiency in specific fuel consumption rate ranges.

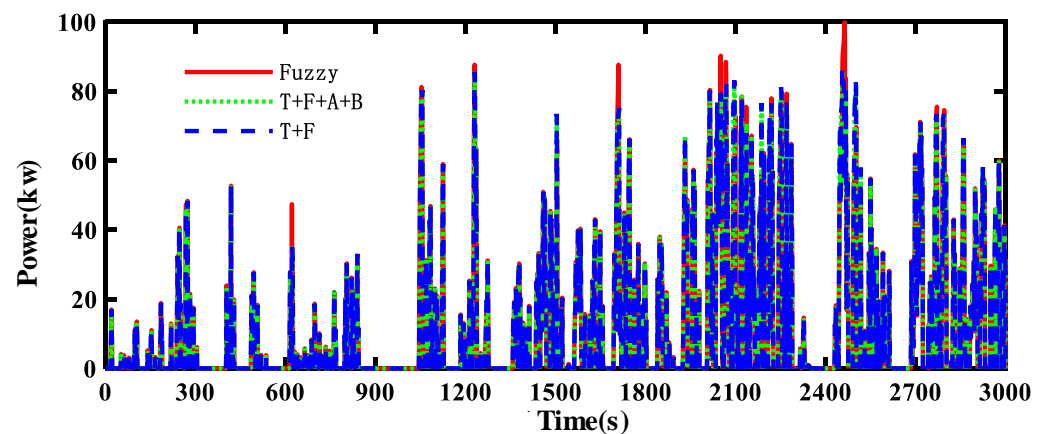


Figure 15. Engine power under three strategies.

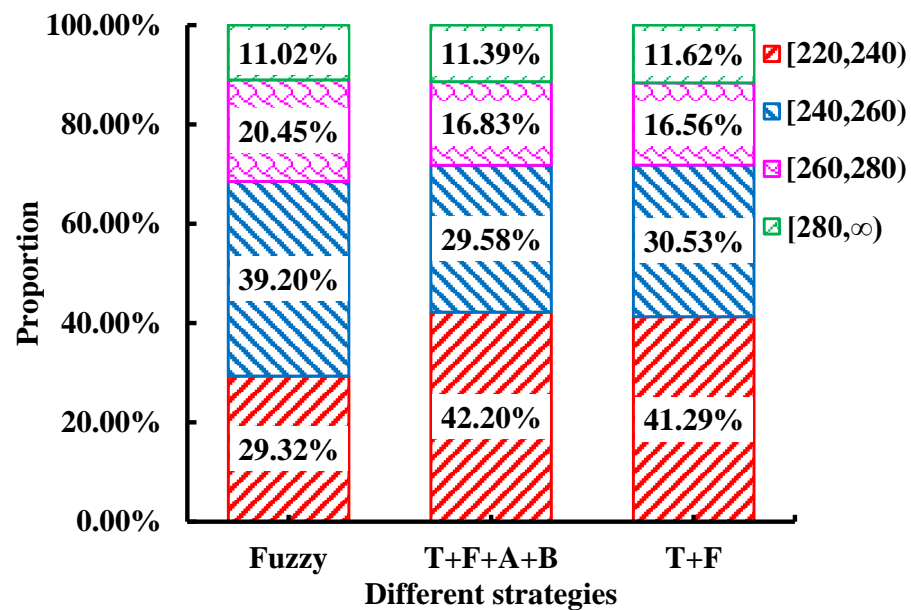


Figure 16. Engine fuel consumption rate distribution under different strategies.

5. Conclusions

The objective of the energy management strategy for hybrid energy storage systems in extended-range electric vehicles is to efficiently allocate energy to achieve optimal fuel economy. The energy storage control system effectively manages energy sources based on real-time traffic information and the current vehicle status obtained from the driving environment. However, vehicles often operate in uncertain and variable conditions, introducing challenges for energy management strategies to adapt quickly to sudden changes. To address these challenges, we introduce a working condition pattern recognition method. We combine this method with a practical fuzzy control strategy for real-time applications, allowing us to optimize parameters for different operating conditions. From our analysis, the following conclusions can be drawn:

(1) The optimal estimate for time-frequency-domain features is found to be seven. The recognition rate decreases as the update time increases. Longer update times show a trend where the recognition rate initially increases and then decreases as the estimated number increases. This suggests that the impact of update time on the recognition rate increases with the estimated number, with an initial increase, a subsequent decrease, and then a small increase. As update time increases, the degree of overfitting also increases, with the trend initially decreasing and then increasing with an increasing estimate number.

(2) When employing an identical recognition step size, long short-term memory (LSTM) surpasses the extreme learning machine (ELM) in recognition accuracy while concurrently demonstrating reduced levels of overfitting. Consequently, LSTM showcases superior recognition performance in comparison to ELM.

(3) The addition of time-frequency features, accelerator pedal signals, and brake pedal signals to the time-domain features has varying effects on the recognition rate. Time-frequency-domain features have the most significant impact, followed by accelerator pedal signals, while brake pedal signals have the smallest impact. Combining time-frequency-domain features, accelerator pedal signals, and brake pedal signals comprehensively yields the most substantial improvement in recognition efficiency. The fusion of diverse feature types for working condition identification can further enhance the recognition rate.

(4) Incorporating fuzzy energy management strategies after integrating working condition identification can further enhance fuel economy. Among the various working condition identification methods using different types of characteristics, the fuzzy energy management strategy utilizing multi-dimensional characteristics, including time domain, time-frequency domain, accelerator pedal signals, and brake pedal signals, performs the best.

Author Contributions: Conceptualization, C.W.; methodology, C.W. software, C.W. and X.W.; validation, Y.C. (Yong Chen), Y.C. (Yunxing Chen) and H.W. Writing of the manuscript: C.W. All authors have read and agreed to the published version of the manuscript.

Funding: This work was supported in part by the Ningbo Science and technology project of China (No. 2019B10111) and the National Key R&D Program of China (No. 2018YFB0106403).

Data Availability Statement: Not applicable.

Conflicts of Interest: The authors declare no conflict of interest.

Abbreviations

EMS	Energy Management Strategy	GIS	Geographical Information Systems
ERELV	Extended-Range Electric Logistics Vehicle	ELM	Extreme Learning Machine
GPS	Global Positioning Systems		
DP	Dynamic Programming	RB-EMS	Rule-based Energy Management Strategy
DPR	Driving Pattern Recognition	SOC	State of Charge
LSTM	Long Short-Term Memory Neural Network	PHEV	Plug-in Hybrid Electric Vehicle
ITS	Intelligent Transportation Systems	VMD	Variational Mode Decomposition Algorithm

Nomenclature

η_T	Transmission Efficiency	r_{roll}	Rolling Radius
i_T	Transmission Ratio	Q_e	Fuel Consumption
T_p	Driving Torque	$T_E(t), \omega_E(t)$	Engine Torque and Speed
T_b	Brake Torque	$b_E(t)$	Engine Fuel Consumption Rate
m	Overall Mass of Vehicle	ρ_f	Fuel Specific Gravity
δ	Rotational Mass Coefficient	η_M	Electrical Circuitry Efficiency
v	Vehicle Speed	U_{VOC}	Open Circuit Voltage
ρ_a	Air Density	ω_k	Mode Center Frequency
α	Road Slope	$\hat{u}_k^{n+1}(\omega)$	Fourier Transform Component
f	Coefficient of Rolling Resistance	W_i, W_f, W_a	Input Weight Vector
C_D	Air Resistance Coefficient	u_f	Fuzzy Controller Output
S	Wind Area	r_{roll}	Rolling Radius

References

- Guo, J.; Wang, J.; Xu, Q.; Wang, B.; Li, K. Deep Reinforcement Learning-based Hierarchical Energy Control Strategy of a Platoon of Connected Hybrid Electric Vehicles through Cloud Platform. *IEEE Trans. Transp. Electr.* **2023**. [\[CrossRef\]](#)
- Wu, L.; Lyu, Z.; Huang, Z.; Zhang, C.; Wei, C. Physics-based battery SOC estimation methods: Recent advances and future perspectives. *J. Energy Chem.* **2023**. [\[CrossRef\]](#)
- Li, Y.; Hu, Z.; Liu, H.; Xu, L.; Li, J.; Xu, L.; Ouyang, M. Comprehensive analysis of cathode air pressure of fuel cell powertrain system of aircraft: Performance, efficiency, and control. *Energy Convers. Manag.* **2023**, *283*, 116903. [\[CrossRef\]](#)
- Wei, C.; Sun, X.; Chen, Y.; Zang, L.; Bai, S. Comparison of architecture and adaptive energy management strategy for plug-in hybrid electric logistics vehicle. *Energy* **2021**, *230*, 120858. [\[CrossRef\]](#)
- Xiao, B.; Walker, P.D.; Zhou, S.; Yang, W.; Zhang, N. A power consumption and total cost of ownership analysis of extended range system for a logistics van. *IEEE Trans. Transp. Electr.* **2021**, *8*, 72–81. [\[CrossRef\]](#)
- Xiao, B.; Yang, W.; Wu, J.; Walker, P.D.; Zhang, N. Energy management strategy via maximum entropy reinforcement learning for an extended range logistics vehicle. *Energy* **2022**, *253*, 124105. [\[CrossRef\]](#)
- Rahman, K.M.; Jurkovic, S.; Stancu, C.; Morgante, J.; Savagian, P.J. Design and performance of electrical propulsion system of extended range electric vehicle (EREV) chevrolet volt. *IEEE Trans. Ind. Appl.* **2014**, *51*, 2479–2488. [\[CrossRef\]](#)
- Taherzadeh, E.; Hamid, R.; Ali, M.S. A comprehensive study of the parameters impacting the fuel economy of plug-in hybrid electric vehicles. *IEEE Trans. Intell. Veh.* **2020**, *5*, 596–615. [\[CrossRef\]](#)
- Xiao, B.; Ruan, J.; Yang, W.; Walker, P.; Zhang, N. A review of pivotal energy management strategies for extended range electric vehicles. *Renew. Sustain. Energy Rev.* **2021**, *149*, 111194. [\[CrossRef\]](#)
- Hu, D.; Xie, H.; Song, K.; Zhang, Y.; Yan, L. An apprenticeship-reinforcement learning scheme based on expert demonstrations for energy management strategy of hybrid electric vehicles. *Appl. Energy* **2023**, *342*, 121227. [\[CrossRef\]](#)

11. Yan, M.; Xu, H.; Li, M.; He, H.; Bai, Y. Hierarchical predictive energy management strategy for fuel cell buses entering bus stops scenario. *Green Energy Intell. Transp.* **2023**, *2*, 100095. [[CrossRef](#)]
12. Zhang, Y.; Gao, B.; Jiang, J.; Liu, C.; Zhao, D.; Zhou, Q.; Chen, Z.; Lei, Z. Cooperative power management for range extended electric vehicle based on internet of vehicles. *Energy* **2023**, *273*, 127238. [[CrossRef](#)]
13. Kim, M.; Jung, D.; Min, K. Hybrid thermostat strategy for enhancing fuel economy of series hybrid intracity bus. *IEEE Trans. Veh. Technol.* **2014**, *63*, 3569–3579. [[CrossRef](#)]
14. Shabbir, W.; Evangelou, S.A. Threshold-changing control strategy for series hybrid electric vehicles. *Appl. Energy* **2019**, *235*, 761–775. [[CrossRef](#)]
15. Denis, N.; Dubois, M.R.; Trovao, J.P.F.; Desrochers, A. Power split strategy optimization of a plug-in parallel hybrid electric vehicle. *IEEE Trans. Veh. Technol.* **2017**, *67*, 315–326. [[CrossRef](#)]
16. Chen, B.-C.; Wu, Y.-Y.; Tsai, H.-C. Design and analysis of power management strategy for range extended electric vehicle using dynamic programming. *Appl. Energy* **2014**, *113*, 1764–1774. [[CrossRef](#)]
17. Peng, J.; He, H.; Xiong, R. Rule based energy management strategy for a series-parallel plug-in hybrid electric bus optimized by dynamic programming. *Appl. Energy* **2017**, *185*, 1633–1643. [[CrossRef](#)]
18. Yu, X.; Lin, C.; Zhao, M.; Yi, J.; Su, Y.; Liu, H. Optimal energy management strategy of a novel hybrid dual-motor transmission system for electric vehicles. *Appl. Energy* **2022**, *321*, 119395. [[CrossRef](#)]
19. Saiteja, P.; Ashok, B. Critical review on structural architecture, energy control strategies and development process towards optimal energy management in hybrid vehicles. *Renew. Sustain. Energy Rev.* **2022**, *157*, 112038. [[CrossRef](#)]
20. Yang, Y.; Bremner, S.; Menictas, C.; Kay, M. Modelling and optimal energy management for battery energy storage systems in renewable energy systems: A review. *Renew. Sustain. Energy Rev.* **2022**, *167*, 112671. [[CrossRef](#)]
21. Yang, Y.; Bremner, S.; Menictas, C.; Kay, M. Numerical investigation on fuzzy logic control energy management strategy of parallel hybrid electric vehicle. *Energy Procedia* **2019**, *158*, 2643–2648.
22. Shen, Y.; Li, Y.; Tang, Y.; Sun, J.; Zhao, J.; Yang, X. An energy management strategy based on fuzzy logic for hybrid energy storage system in electric vehicles. *IEEJ Trans. Electr. Electron. Eng.* **2022**, *17*, 53–60. [[CrossRef](#)]
23. Marzougui, H.; Kadri, A.; Martin, J.-P.; Amari, M.; Pierfederici, S.; Bacha, F. Implementation of energy management strategy of hybrid power source for electrical vehicle. *Energy Convers. Manag.* **2019**, *195*, 830–843. [[CrossRef](#)]
24. Wei, C.; Chen, Y.; Li, X.; Lin, X. Integrating intelligent driving pattern recognition with adaptive energy management strategy for extender range electric logistics vehicle. *Energy* **2022**, *247*, 123478. [[CrossRef](#)]
25. Yang, Y.; Zhang, Y.; Tian, J.; Li, T. Adaptive real-time optimal energy management strategy for extender range electric vehicle. *Energy* **2020**, *197*, 117237. [[CrossRef](#)]
26. Vatanparvar, K.; Faezi, S.; Burago, I.; Levorato, M.; Al Faruque, M.A. Extended range electric vehicle with driving behavior estimation in energy management. *IEEE Trans. Smart Grid* **2018**, *10*, 2959–2968. [[CrossRef](#)]
27. Yao, M.; Zhu, B.; Zhang, N. Adaptive real-time optimal control for energy management strategy of extended range electric vehicle. *Energy Convers. Manag.* **2021**, *234*, 113874. [[CrossRef](#)]
28. Zhu, D.; Pritchard, E.; Dadam, S.R.; Kumar, V.; Xu, Y. Optimization of rule-based energy management strategies for hybrid vehicles using dynamic programming. *arXiv* **2022**, arXiv:2207.06450. [[CrossRef](#)]
29. Zeng, P.; Li, H.; He, H.; Li, S. Dynamic energy management of a microgrid using approximate dynamic programming and deep recurrent neural network learning. *IEEE Trans. Smart Grid* **2018**, *10*, 4435–4445. [[CrossRef](#)]
30. Li, J.; Song, Z.; Wang, X.; Wang, Y.; Jia, Y. A novel offshore wind farm typhoon wind speed prediction model based on PSO-Bi-LSTM improved by VMD. *Energy* **2022**, *251*, 123848. [[CrossRef](#)]
31. Zhao, L.; Li, Z.; Qu, L.; Zhang, J.; Teng, B. A hybrid VMD-LSTM/GRU model to predict non-stationary and irregular waves on the east coast of China. *Ocean. Eng.* **2023**, *276*, 114136. [[CrossRef](#)]
32. Cheng, Z.; Chen, B.; Lu, R.; Wang, Z.; Zhang, H.; Meng, Z.; Yuan, X. Recurrent neural networks for snapshot compressive imaging. *IEEE Trans. Pattern Anal. Mach. Intell.* **2022**, *45*, 2264–2281. [[CrossRef](#)] [[PubMed](#)]
33. Ewees, A.A.; Mohammed, A.A.; Laith, A.; Elaziz, M.A. HBO-LSTM: Optimized long short term memory with heap-based optimizer for wind power forecasting. *Energy Convers. Manag.* **2022**, *268*, 116022. [[CrossRef](#)]
34. Granata, F.; Fabio, D.N.; Giovanni, D.M. Stacked machine learning algorithms and bidirectional long short-term memory networks for multi-step ahead streamflow forecasting: A comparative study. *J. Hydrol.* **2022**, *613*, 128431. [[CrossRef](#)]
35. Pan, Y.G.; Wu, Y.M.; Lam, H.-K. Security-based fuzzy control for nonlinear networked control systems with DoS attacks via a resilient event-triggered scheme. *IEEE Trans. Fuzzy Syst.* **2022**, *30*, 4359–4368. [[CrossRef](#)]
36. Lin, H.; Han, Y.; Cai, W.; Jin, B. Traffic signal optimization based on fuzzy control and differential evolution algorithm. *IEEE Trans. Intell. Transp. Syst.* **2022**, *24*, 8555–8566. [[CrossRef](#)]
37. Liu, H.; Zhao, J.Y.; Qing, T.; Li, X. Energy consumption analysis of a parallel PHEV with different configurations based on a typical driving cycle. *Energy Rep.* **2021**, *7*, 254–265. [[CrossRef](#)]

Disclaimer/Publisher's Note: The statements, opinions and data contained in all publications are solely those of the individual author(s) and contributor(s) and not of MDPI and/or the editor(s). MDPI and/or the editor(s) disclaim responsibility for any injury to people or property resulting from any ideas, methods, instructions or products referred to in the content.